Differential effects of the proteasome inhibitor bortezomib on apoptosis and angiogenesis in human prostate tumor xenografts

Simon Williams,[1] Curtis Pettaway,[1,2]
Rendu Song,[2] Christos Papandreou,[3]
Christopher Logothetis,[3] and
David J. McConkey[1]

Departments of [1]Cancer Biology, [2]Urology, and [3]Genitourinary Medical Oncology, The University of Texas M.D. Anderson Cancer Center, Houston, TX

Abstract

Bortezomib (Velcade, PS-341) is a dipeptide boronate inhibitor of the 26S proteasome developed for use in cancer therapy. Here we examined the effects of bortezomib on apoptosis and angiogenesis in derivatives of two popular human prostate cancer cell lines (LNCaP-Pro5 and PC3M-Pro4). Bortezomib strongly inhibited proliferation in both cell lines *in vitro*, but the PC3M-Pro4 cells were significantly more sensitive than the LNCaP-Pro5 cells to bortezomib-induced apoptosis. The compound also significantly inhibited the growth of LNCaP-Pro5 and LNCaP-Pro4 tumor xenografts, but the mechanisms involved in tumor growth inhibition differed in the two models. Bortezomib-treated LNCaP-Pro5 tumors displayed reduced microvessel densities and vascular endothelial cell growth factor secretion and high levels of endothelial cell apoptosis consistent with angiogenesis inhibition. In contrast, PC3M-Pro4 tumors were poorly vascularized at baseline, and bortezomib failed to induce significant changes in microvessel density, angiogenic factor secretion, or endothelial cell death in this model. Rather, growth inhibition in the PC3M-Pro4 tumors was associated with direct increases in tumor cell death. Together, our results confirm that bortezomib is active in preclinical models of human prostate cancer, but its effects on apoptosis *versus* angiogenesis are cell type dependent. (Mol Cancer Ther. 2003;2:835–843)

Introduction

Although early detection has improved the prognosis for a large fraction of patients with prostate cancer, control of disseminated disease remains a major therapeutic challenge. Androgen ablation is initially extremely effective in reducing disease burden, but patients inevitably relapse with hormone-insensitive disease that appears to be largely refractory to a variety of different conventional regimens. Thus, there is currently a strong push to develop compounds that interact with novel biological targets, either for use as single agents or perhaps more commonly in combination with front-line chemo- and radiotherapy. Unfortunately, our understanding of basic biology in prostate cancer is far from complete, and it is therefore difficult at present to predict which patients would benefit from investigational biological agents.

The 26S proteasome is a large, multicatalytic structure responsible for degrading a number of different polypeptides important for cell cycle progression and cell survival (1–3). The subunits of the proteasome are structurally conserved through evolution (4), and complete loss-of-function mutations in the subunits are lethal, indicating that normal proteasome function plays a requisite role in normal cell physiology. Interestingly, however, recent studies demonstrated that proteasome inhibitors are much more active in tumor cells compared to their normal counterparts (5, 6), and in some cases, proteasome inhibitors actually delay or prevent programmed cell death (7, 8). These observations stimulated the development of bortezomib (Velcade, previously PS-341) for cancer therapy in humans (9–12). Bortezomib exhibited excellent activity in the National Cancer Institute's panel of 60 cell lines, with a mean IC_{50} across the panel of 7 nM (9). More importantly, its activity was unlike that of any other class of compounds examined in the screen ($n > 100,000$) (9), strongly suggesting that it interacted with a unique biological target. Preclinical studies confirmed that the drug was active in tumor xenografts (9, 13–16), and bortezomib is currently being evaluated in a series of Phase I–III clinical trials in patients with a variety of solid and hematological malignancies (11). Importantly, there is significant interest in developing bortezomib for the therapy of androgen-independent prostate cancer because of promising activity observed in the studies conducted to date.

Here we examined the effects of bortezomib on the growth of *in vivo*-selected derivatives of two popular human prostate cancer cell lines (LNCaP and PC-3). LNCaP-Pro5 was selected by orthotopic "recycling" for aggressive local growth within the prostate and retains many features of early-stage disease (androgen-sensitive, wild-type p53, nonmetastatic) (17). In contrast, PC3M-Pro4 was derived from the highly metastatic PC-3M subline, and it is not only locally aggressive but also highly metastatic (17). PC3M-Pro4 is androgen receptor-and p53-negative and is completely androgen independent *in vitro* and *in vivo*. Our overall goal was to evaluate the activity of bortezomib in disparate prostate cancer models and to characterize the biological mechanisms involved in whatever tumor growth inhibition was observed.

Materials and Methods

Cell Culture and Reagents

The LNCaP-Pro5 and PC3M-Pro4 human prostatic adenocarcinoma cell lines were developed as described previously(17). They were maintained in RPMI supplemented with 10% FCS, antibiotics, vitamins, and pyruvate under an atmosphere of 5% CO_2.

MTT Assays

Cells were cultured in 96-well plates at a concentration of 10,000 cells/well and left to recover (LNCaP-Pro5: 48 h, PC3M-Pro4: 24 h). Cells were exposed to bortezomib for 48 h, drug was removed, and cells were cultured in drug-free medium overnight. Cells were then incubated with MTT (3-[4,5-dimethylthiazol-2-yl]-2,5-diphenyltetrazolium bromide in PBS at 5 mg/ml, Sigma Chemical Co., St. Louis, MO) (10 μl/well) for 2 h (37°C). The medium was replaced with DMSO (40 μl/well) and MTT precipitates were dissolved for 1 h before quantification of optical densities (570 nm).

Propidium Iodide and Fluorescence-Activated Cell Sorting Analysis

Cells were incubated with bortezomib for 48 h and harvested by trypsinization. The trypsinized cells, media, and PBS wash were mixed and centrifuged. Supernatants were removed and the cells were resuspended in 400 μl of a cold (4°C) propidium iodide solution (50 μg/ml propidium iodide, 0.1% Triton X-100, and 0.1% sodium citrate, in PBS). Cells were incubated in the solution for at least 2 h at 4°C before analysis by flow cytometry. Cells with a subdiploid DNA content were scored as apoptotic (% sub-G_0/G_1) as described previously (18).

Caspase 3 Activation

Cells were split to 10-cm plates and left to recover for 48 h before treatment. After treatment, cells were harvested by trypsinization, and the trypsinized cells, the media, and the PBS washes were added together and collected by centrifugation. The cells were washed in cold PBS, resuspended in 500 μl of a 2% solution of paraformaldehyde in PBS, and left on ice for 20 min. The cells were then pelleted and resuspended in a 0.2% solution of Triton X-100 in PBS and left on ice for 5 min. One milliliter of cold fluorescence-activated cell sorting (FACS) buffer was then added (1% sodium azide, 2% fetal bovine serum in PBS). The cells were then pelleted and washed again in FACS buffer. The cells were then resuspended in 50 μl of FACS buffer containing 20 μl phycoerythrin (PE)-conjugated anti-active caspase 3 antibody (BD Biosciences, Palo Alto, CA), and samples were incubated for 30 min on ice. Samples were washed twice in FACS buffer, resuspended in 500 μl FACS buffer, and analyzed by flow cytometry. The proportion of cells staining for PE above the levels of a nonspecific PE-conjugated control antibody (PE-conjugated anti-mouse Ig, κ light chain, PharMingen, Palo Alto, CA) was quantified.

Analysis of Phosphatidylserine Exposure by Annexin V Staining

Annexin V staining was conducted with the use of a kit (Annexin V-PE apoptosis detection kit I, BD Biosciences). Cells were split to 10-cm plates and left to recover for 24 (PC3M-Pro4) or 48 (LNCaP-Pro5) h before exposure to bortezomib. After treatment, cells were harvested by trypsinization, and the trypsinized cells, the media, and the PBS wash were added together and collected. The cells were washed twice in cold PBS and resuspended in 100 μl of binding buffer (supplied by the vendor) containing 5 μl PE-conjugated annexin V. Cells were incubated for 15 min on ice, and 400 μl of binding buffer was added to each sample before analysis by flow cytometry.

Secretion of Angiogenic Factors *in Vitro*

Cells were incubated in a conventional incubator or in a hypoxia chamber (1% O_2) for the times indicated in the absence or presence of bortezomib. Conditioned media were collected and frozen at −20°C. Factor production in the supernatants was quantified by ELISA using commercial kits specific for vascular endothelial cell growth factor (VEGF), basic fibroblast growth factor (bFGF), or interleukin-8 (IL-8) (R&D Systems, Minneapolis, MN) following product protocols. The colorimetric readings at 450 nm were normalized to the cell counts.

Tumor Xenografts

PC3M-Pro4 and LNCaP-Pro5 cells were mixed with Matrigel (Becton Dickinson Labware, Bedford, MA) (1×10^6 cells in 200 μl) and injected into each flank of 6-week-old male nude mice (BALB/c background, purchased from the Animal Production Area of the National Cancer Institute-Frederick Cancer Research and Development Center, Frederick, MD). Tumors were established for 2 weeks before the start of treatment. Mice were subjected to a course of six tail vein injections of 1 mg/kg bortezomib in 20 μl of saline or 20 μl saline alone (controls) every 72 h. Tumor measurements (the longest and shortest tumor diameters) were performed at the time of each injection. Tumor volumes were calculated according to the following formula: volume = $(l)(w^2/2)$, where l = length and w = width. Mice were euthanized by cervical dislocation 24 h after the last injection. The tumors were harvested and either fixed in formaldehyde and embedded in paraffin or immersed in OCT compound (Optimal Cutting Temperature, Sakura Finetechnical Co., Torrance, CA) and frozen in liquid nitrogen.

Immunofluorescence Analyses

Tumor sections on charged slides were deparafinized and subjected to staining for cellular morphology with H&E, and for proliferating cell nuclear antigen (PCNA) (primary antibody, mouse monoclonal, DAKO, Carpinteria, CA; secondary antibody, Alexa 488-conjugated rabbit polyclonal, Molecular Probes, Eugene, OR), VEGF (primary antibody, rabbit polyclonal, Santa Cruz Biotechnology, Santa Cruz, CA; secondary antibody, FITC-conjugated goat polyclonal, The Jackson Laboratory, Bar Harbor, ME), bFGF (primary antibody, rabbit polyclonal, Sigma; secondary antibody: FITC-conjugated goat polyclonal, The Jackson Laboratory), and IL-8 (primary antibody, rabbit polyclonal, Biosource International, Camarillo, CA; secondary antibody, FITC-conjugated goat

polyclonal, The Jackson Laboratory). Tissues were washed twice in PBS and circled with a pap pen before the slides were transferred to humidity chambers. Slides were incubated in protein blocking solution (5% normal horse serum, 1% goat serum in PBS) for 20 min before the addition of the primary antibody (diluted in blocking solution), which was left on the tissues overnight at 4°C. Tissues were then washed 3× in PBS and blocked for 10 min before incubation with secondary antibodies in blocking solution for 1 h. This and subsequent steps were conducted in the dark. Sections were washed twice in PBS before they were counterstained with 1 μg/ml propidium iodide in PBS for 10 min. Sections were washed 3×, and Prolong antifade mounting agent (Molecular Probes) and a cover slide were added to each. Images were captured with an Axioplan 2 microscope, a Hamamatsu color chilled 3CCD camera, and Optimus software (Bioscan, Edmonds, WA).

Detection of Tumor Microvessels

Frozen tissue sections were fixed in acetone, washed in PBS, and blocked for endogenous peroxidase activity with a 3% hydrogen peroxide solution in methanol for 12 min. Sections were then washed in PBS and incubated in protein blocking solution for 20 min. Slides were incubated overnight at 4°C with anti-CD31 primary antibody (rat polyclonal, Pharmacia, Piscataway, NJ) in protein blocking solution. The primary antibody was removed, sections were washed in PBS and blocked for 10 min, and tissues were incubated for 1 h at room temperature with the secondary antibody (goat polyclonal horseradish peroxidase-conjugated, The Jackson Laboratory). Sections were washed in PBS, and positive staining was visualized by incubating the slides with stable 3,3′-diaminobenzidine for 10–20 min. The sections were rinsed with distilled water, counterstained with Gill's hematoxylin (colorimetric development), and mounted with Universal Mount (Research Genetics, Huntsville, AL). Control samples exposed to secondary antibody alone showed no specific staining.

In Vivo Measurement of Apoptosis

Frozen tissue sections were fixed in acetone, washed in PBS, and blocked for 20 min before they were incubated with anti-CD31 primary antibody (rat polyclonal, Pharmacia) in blocking solution overnight at 4°C. Tissues were washed in PBS, blocked for 10 min, and incubated with the secondary antibody (Cy5-conjugated goat polyclonal, The Jackson Laboratory) for 1 h. This and subsequent steps were conducted in the dark. Sections were then washed with PBS and treated with a 4% formaldehyde solution in PBS for 10 min. Slides were washed, incubated with 0.2% Triton X-100 for 15 min, and washed again. DNA fragmentation was visualized by staining tissue sections with a commercial kit (Dead-End fluorometric TUNEL system, Promega, Madison, WI). Tissues were incubated in equilibration buffer for 10 min before the addition of the reaction cocktail containing terminal dNTP transferase and FITC-conjugated nucleotides. Slides were incubated for 1 h at 37°C, and reactions were terminated by incubation in 2× SSC for 15

min. Tissues were washed in PBS and counterstained with a 1 μg/ml solution of propidium iodide in PBS for 10 min. After a final round of washes, slides were mounted with Prolong (Molecular Probes) and cover slides. Images were captured with an Axioplan 2 microscope, a Hamamatsu color chilled 3CCD camera, and Optimus software (Bioscan). TUNEL-positive cells were quantified by laser scanning cytometry (LSC; Compucyte, Cambridge, MA) (15, 19).

Results

Concentration-Dependent Effects of Bortezomib on Cell Proliferation and Apoptosis *in Vitro*

In a previous study with the National Cancer Institute's panel of 60 human cell lines, bortezomib displayed a mean IC_{50} of 7 nM as determined by SRB analysis (9). Similarly, bortezomib caused comparable, concentration-dependent growth suppression in LNCaP-Pro5 and PC3M-Pro4 cells (IC_{90} = 10 nM) (Fig. 1A). These effects were associated with DNA fragmentation typical of apoptosis as measured by propidium iodide staining and FACS analysis (Fig. 1B). However, PC3M-Pro4 cells displayed significant DNA fragmentation (60%) at bortezomib concentrations as low as 10 nM, whereas higher concentrations of drug were required to stimulate significant DNA fragmentation in LNCaP-Pro5 cells (Fig. 1B). A maximally effective concentration of bortezomib (1 μM) stimulated DNA fragmentation in both cell lines, although the levels observed in PC3M-Pro4 cells were significantly higher than the levels observed in LNCaP-Pro5 cells (Fig. 1B). The involvement of apoptosis in bortezomib-induced cell killing was confirmed in both cell lines via analysis of phosphatidylserine exposure (Fig. 1C) and activation of caspase-3 (Fig. 1D). Again, the absolute levels of apoptosis in PC3M-Pro4 cells were somewhat higher than the levels observed in LNCaP-Pro5 cells. The results of these studies confirmed that bortezomib stimulated substantial levels of apoptosis in both cell lines *in vitro*, although the PC3M-Pro4 cells displayed higher sensitivity in all three assays, especially at clinically relevant concentrations of drug (10 nM).

Effects of Bortezomib on Tumor Growth *in Vivo*

Previous studies demonstrated that maximally tolerated doses of bortezomib (1 mg/kg) produced significant growth inhibition in several different human tumor xenograft models *in vivo* (9, 14, 15). We therefore compared the activity of this dose of bortezomib in s.c. LNCaP-Pro5 and PC3M-Pro4 tumors (1 mg/kg every 72 h for a total of six i.v. injections). This schedule was chosen to allow recovery of 20S proteasome activity to normal levels before each dose of drug (9). Bortezomib inhibited the growth rates of both types of tumor (Fig. 2A). The effects of the drug were more pronounced in the LNCaP-Pro5 tumors (80% growth inhibition) as compared with the PC3M-Pro4 tumors (50% growth inhibition) (P 7< 0.05). Gross morphological analyses of the tumors by
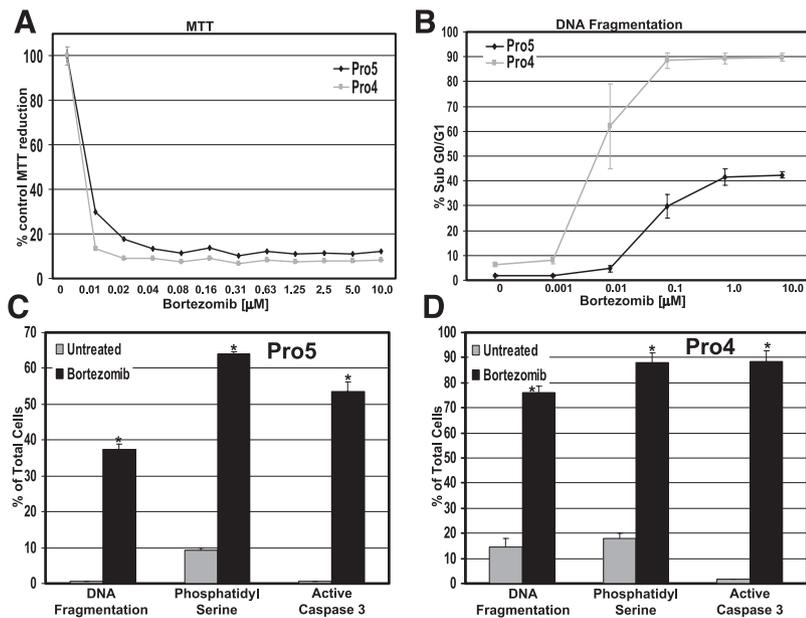
Figure 1. Bortezomib-induced apoptosis in human prostatic carcinoma cells. LNCaP-Pro5 and PC3M-Pro4 cells were treated for 48 h with bortezomib, and various assays were used to measure proliferation and apoptosis. **A,** effects of bortezomib on proliferation. Cells were incubated with various concentrations of drug as described in ''Materials and Methods.'' Mean values from eight replicate samples. Results of one experiment representative of three independent replicates. **B,** effects of bortezomib on DNA fragmentation. Cells were incubated in the presence of the indicated concentrations of bortezomib, and DNA fragmentation was measured by propidium iodide staining and FACS analysis as described in ''Materials and Methods.'' Mean $\pm$ SD, $n = 3$. *, $P < 0.05$. **C** and **D**, effects of bortezomib phosphatidylserine (*PS*) exposure and caspase activation. Cells were treated with 1 μM bortezomib for 48 h, and phosphatidylserine exposure and active caspase-3 levels were measured by flow cytometry as described in ''Materials and Methods.'' **C,** LNCaP-Pro5 cells. **D,** PC3M-Pro4 cells. Mean $\pm$ SD, $n = 3$. *, $P < 0.05$, bortezomib *versus* controls; PC3M-Pro4 *versus* LNCaP-Pro5.

H&E staining revealed substantial necrosis, particularly in the PC3M-Pro4-derived tumors (Fig. 2B). Consistent with the results of the MTT studies, the bortezomib-treated tumors displayed much lower levels of PCNA compared to the controls (Fig. 2C). Quantitative analyses of tumor cell death by TUNEL staining and LSC analysis demonstrated that bortezomib stimulated significant increases in apoptosis in PC3M-Pro4 and LNCaP-Pro5 tumors (Fig. 3, A and B).

Effects of Bortezomib on Angiogenic Factor Production

Recent studies demonstrated that bortezomib-induced tumor growth inhibition was associated with inhibition of angiogenesis in other tumor model systems (14, 15). To investigate possible effects of bortezomib on angiogenesis in our models, we incubated LNCaP-Pro5 or PC3M-Pro4 cells with 1 μM bortezomib and quantified the levels of VEGF, IL-8, and bFGF in conditioned medium by ELISA. At baseline, the LNCaP-Pro5 cells secreted high levels of VEGF but not IL-8 or bFGF, whereas the PC3M-Pro4 cells secreted relatively modest levels of all three cytokines (Fig. 4A). Exposure to hypoxia produced time-dependent increases in VEGF secretion (but not IL-8 or bFGF secretion, data not shown) in the LNCaP-Pro5 cells (Fig. 4B) but it had no effect on VEGF secretion by the PC3M-Pro4 cells (data not shown). Consistent with these results, LNCaP-Pro5 tumors expressed high levels of VEGF (Fig. 4C) (but not IL-8 or bFGF) (Fig. 4, D and E), whereas levels of all three growth factors were very low in PC3M-Pro4 tumors (Fig. 4, C–E). Bortezomib strongly inhibited hypoxia-induced VEGF secretion in the LNCaP-Pro5 cells (Fig. 4B) but did not further reduce the low-level baseline secretion of IL-8 or bFGF in the LNCaP-Pro5 cells (Fig. 4A). VEGF expression was strongly suppressed in bortezomib-treated LNCaP-Pro5 tumors (Fig. 4C), but the drug had little effect on the low-level expression of IL-8 or bFGF in LNCaP-Pro5 tumors or VEGF, IL-8, or bFGF expression in the PC3M-

Pro4 tumors (Fig. 4, C–E). Together, these data suggest that the LNCaP-Pro5 cells are more angiogenic than the PC3M-Pro4 cells and that angiogenesis in the LNCaP-Pro5 tumors is driven by VEGF.

Effects of Bortezomib on Endothelial Cell Apoptosis

We have shown that tumor growth inhibition induced by antiangiogenic agents is associated with induction of apoptosis in tumor-associated endothelial cells (20–23). To obtain more direct information about the effects of bortezomib on angiogenesis, we stained frozen tissue sections with an antibody to CD31 and measured tumor microvessel densities (MVDs) by manual counting. In untreated conditions, the architecture of microvessels in the LNCaP-Pro5 tumors was very different from that observed in the PC3M-Pro4 xenografts. Vessels in the LNCaP-Pro5 tumors tended to be larger and contain more lumen than the vessels in the PCM-Pro4 tumors (Fig. 5A). Quantitative analyses demonstrated that the LNCaP-Pro5 tumors exhibited higher baseline MVDs than the PC3M-Pro4 tumors (Fig. 5B) ($P < 0.05$). Bortezomib reduced the MVDs in the LNCaP-Pro5 tumors by approximately 40%, whereas it had no effect on the already low MVDs observed in the PC3M-Pro4 tumors (Fig. 5B). We also used two-color fluorescent anti-CD31/TUNEL immunofluorescence in tumor sections counterstained with propidium iodide to quantify the percentages of total tumor-associated cells that were endothelial in origin using the LSC (mean endothelial cell density, MED). The results confirmed that bortezomib produced a significant decrease in tumor-associated endothelial cells in the LNCaP-Pro5 tumors but not in the PC3M-Pro4 xenografts (Fig. 5C). Finally, we characterized the effects of bortezomib on levels of apoptosis in tumor-associated endothelial cells in the anti-CD31/TUNEL-stained sections (Fig. 5D). Quantitative LSC analyses demonstrated that bortezomib produced significant increases in endothelial cell apoptosis in the LNCaP-Pro5
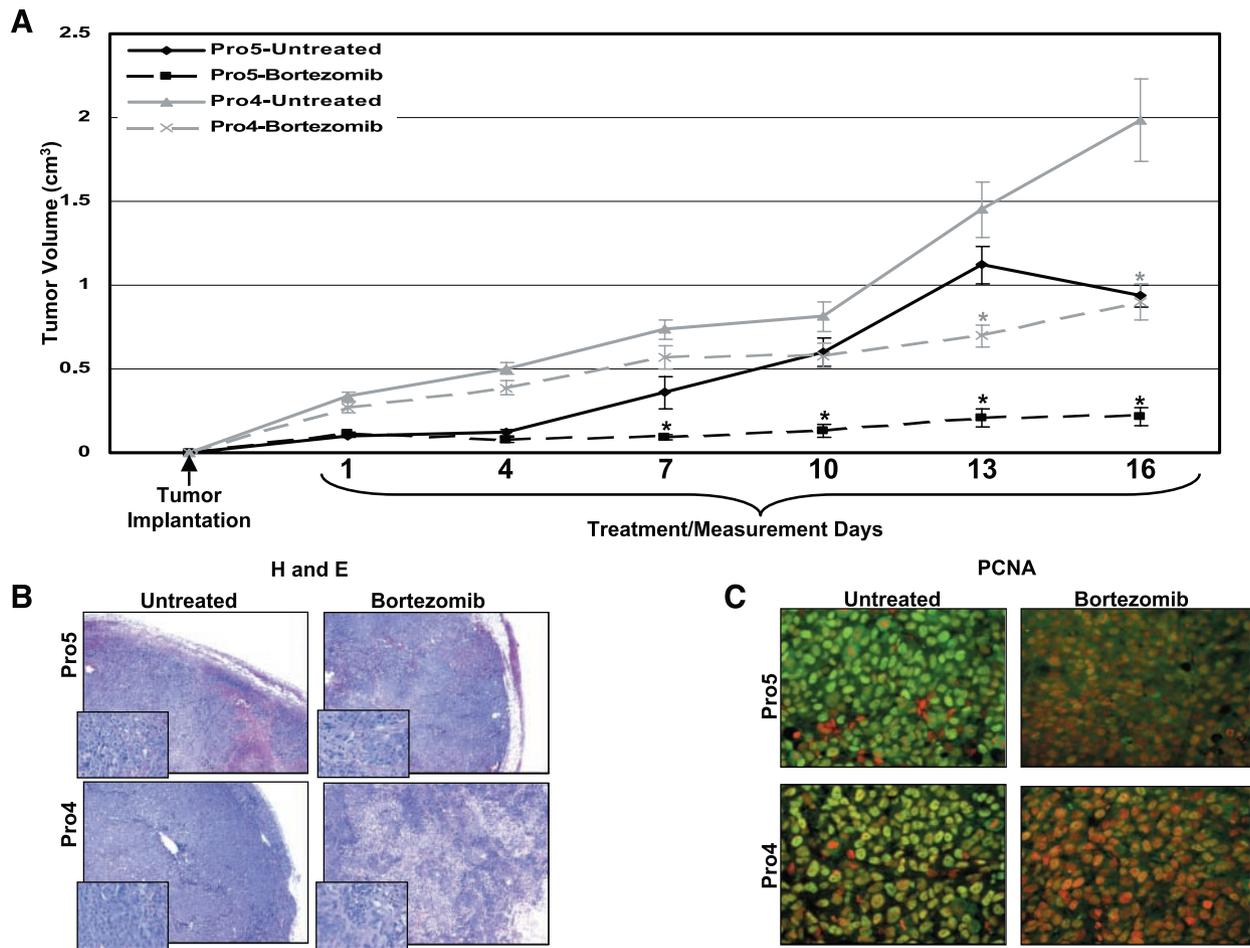
A

B

H and E

C

PCNA

Figure 2. Effects of bortezomib on established LNCaP-Pro5 (*Pro5*) or PC3M-Pro4 (*Pro4*) tumor xenografts. **A,** effects on tumor growth. Subcutaneous tumors were generated by injecting 1×10^6 cells in Matrigel into the flanks of nude mice. Tumors were established for 2 weeks before the initiation of therapy. Tumors were measured throughout the course of therapy and volumes were calculated as described in ''Materials and Methods.'' Mean ± SD, $n = 6$ (LNCaP-Pro5), $n = 10$ (PC3M-Pro4). *, $P < 0.05$. **B,** effects on tumor histology. Representative sections obtained from control or bortezomib-treated LNCaP-Pro5 or PC3M-Pro4 tumors were stained with H&E. *Insets,* higher magnification images of the same conditions. **C,** effects of bortezomib on proliferation. Representative sections obtained from LNCaP-Pro5 or PC3M-Pro4 tumors were stained for PCNA and analyzed by immunofluorescence as described in ''Materials and Methods.''

tumors (3-fold, $P < 0.05$), whereas the levels of endothelial cell death measured in the proteasome inhibitor-treated PC3M-Pro4 tumors were not significantly different from controls (Fig. 5E).

Discussion

Proteasome inhibitors block apoptosis in thymocytes (7) and in primary neuronal cells (8), indicating that the proteasome is required for apoptosis in some normal cell types. Conversely, proteasome inhibitors induce apoptosis in a variety of different tumor cell lines and primary tumor cells (5, 6, 24–27). Thus, even though long-term elimination of proteasome function appears to be incompatible with cell survival, the increased sensitivity of transformed cells to transient proteasome inhibition may provide a manageable therapeutic ''window'' for the use of proteasome

inhibitors in cancer therapy. In 1998, bortezomib (PS-341) became the first drug of its class to undergo human clinical trials, and it is currently being evaluated in a number of different Phase I–III studies in patients with solid and hematological tumors. The drug displays especially promising activity in patients with multiple myeloma, where sustained clinical responses have been observed (11). In patients with androgen-independent prostate cancer, bortezomib produced decreases in prostate specific antigen (PSA, so-called ''PSA responses'') and IL-6 and in a few cases, radiological evidence of disease regression.[1]

The promising results obtained with bortezomib in Phase I prompted us to evaluate its antitumoral activity and mechanisms of action in two human prostate tumor

---

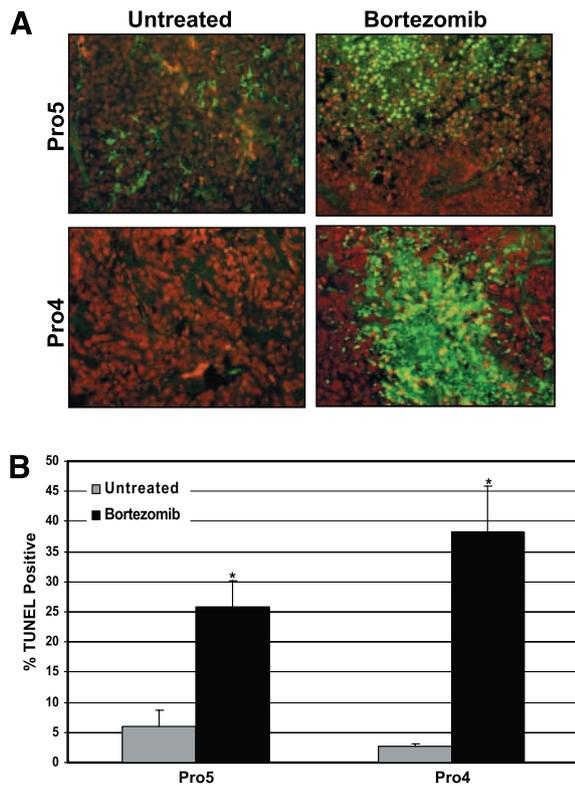[1] C. Papandreou and C. Logothetis, unpublished observations.

Figure 3. Effects of bortezomib on tumor cell apoptosis in LNCaP-Pro5 (*Pro5*) or PC3M-Pro4 (*Pro4*) xenografts. Mice bearing established (14-day) tumors were treated with 1 mg/kg bortezomib i.v. every 72 h (total of six doses), tumors were harvested, and apoptosis was assessed by fluorescent TUNEL as described in ''Materials and Methods.'' **A,** representative TUNEL-stained sections obtained from LNCaP-Pro5 (*top panels*) and PC3M-Pro4 (*lower panels*) tumors. *Green,* TUNEL staining; *red,* propidium iodide staining (total cell nuclei). **B,** quantification of fluorescent TUNEL staining by LSC. Percentages of TUNEL-positive cells were quantified in four independent fields using a laser scanning cytometer as described in ''Materials and Methods.'' Mean ± SD, $n = 10$. *, $P < 0.05$ *versus* controls.

xenografts. Our group developed variants of the popular LNCaP and PC-3M prostate adenocarcinoma lines selected for aggressive growth *in vivo* (17), and we selected these cells for analysis here. In addition, we attempted to generate tumor xenografts using a third human prostate cancer line (DU-145), but the cells were not nearly as tumorigenic as the other lines and the results obtained were impossible to interpret. The results of our MTT experiments demonstrate that bortezomib induces strong growth arrest at clinically relevant concentrations *in vitro* (≤10 nM), and tumor xenografts treated with i.v. bortezomib display substantial inhibition of proliferation (measured by PCNA staining) *in vivo*. However, other aspects of bortezomib's mechanisms of action differ in the two models. In PC3M-Pro4 cells, clinically relevant concentrations of bortezomib induced DNA fragmentation characteristic of apoptosis, whereas higher levels of the drug (1 μM) were required to stimulate apoptosis in the LNCaP-Pro5 cells. Similar patterns were observed in the xenografts, where bortezomib induced higher levels

of TUNEL staining in the PC3M-Pro4 tumors as compared with the levels observed in LNCaP-Pro5 tumors. These results were somewhat surprising given that the PC3M-Pro4 cells are considered much more aggressive than the LNCaP-Pro5 cells. Because proteasome inhibitors appear to preferentially kill cycling cells (6), it is possible that the PC3M-Pro4 cells possess cell cycle checkpoint defect(s) that prevent them from undergoing sustained growth arrest, whereas LNCaP-Pro5 cells do so more efficiently because they possess wild-type p53 and p21. We are currently exploring the role of proteasome inhibitor-mediated cell cycle arrest in resistance to therapy-induced apoptosis in the model systems described here as well as in others. These effects may be especially important when bortezomib is combined with conventional agents (nucleoside analogues, anthracyclines, taxanes) that preferentially target cells at specific stages of the cell cycle.

Although bortezomib induced higher levels of apoptosis in the PC3M-Pro4 cells, bortezomib produced stronger growth inhibition in LNCaP-Pro5 tumors (>70%) as compared to PC3M-Pro4 tumors (approximately 50%). One important mechanism of bortezomib-induced tumor growth inhibition identified in our previous studies and work conducted by others is angiogenesis inhibition. Specifically, we recently showed that bortezomib inhibited VEGF secretion and lowered MVDs in human L3.6pl and Mia PaCa-2 pancreatic tumor xenografts (15), and another group reported similar findings in a model of human squamous cell carcinoma (14). Recent studies indicate that tumors can vary markedly with respect to their dependence on angiogenesis, effects that are linked in part to p53 status. Because p53 appears to mediate hypoxia-induced apoptosis (28), p53-deficient tumors may require fewer blood vessels per unit area to survive and expand (29). As noted above, the LNCaP-Pro5 cells retain wild-type p53, whereas the PC3M-Pro4 cells do not.

Here we demonstrate that the LNCaP-Pro5 cells constitutively secrete very high levels of VEGF that can be increased further by exposing the cells to hypoxia. In contrast, PC3M-Pro4 tumors secrete very low levels of VEGF at baseline, and hypoxia has no effect on VEGF production. Consistent with these *in vitro* findings, LNCaP-Pro5 tumors produce high levels of VEGF and display high MVDs *in vivo*, whereas PC3M-Pro4 tumors produce lower levels of VEGF and display lower MVDs. Bortezomib inhibited baseline and hypoxia-induced VEGF production in LNCaP-Pro5 cells *in vitro* and reduced tumor VEGF expression and MVDs in LNCaP-Pro5 tumors *in vivo*, whereas its effects on angiogenesis in PC3M-Pro4 tumors were much less remarkable. Together, our results strongly suggest that inhibition of tumor angiogenesis plays an important role in the inhibition of LNCaP-Pro5 but not PC3M-Pro4 tumor growth. Nonetheless, our data should not be interpreted to mean that VEGF plays no role in tumor growth and angiogenesis in PC3M-Pro4 tumors. In fact, direct targeting of VEGF-R2/ KDR using a blocking monoclonal antibody (DC-101) (30) or small molecule inhibitors (31, 32) attenuated the growth
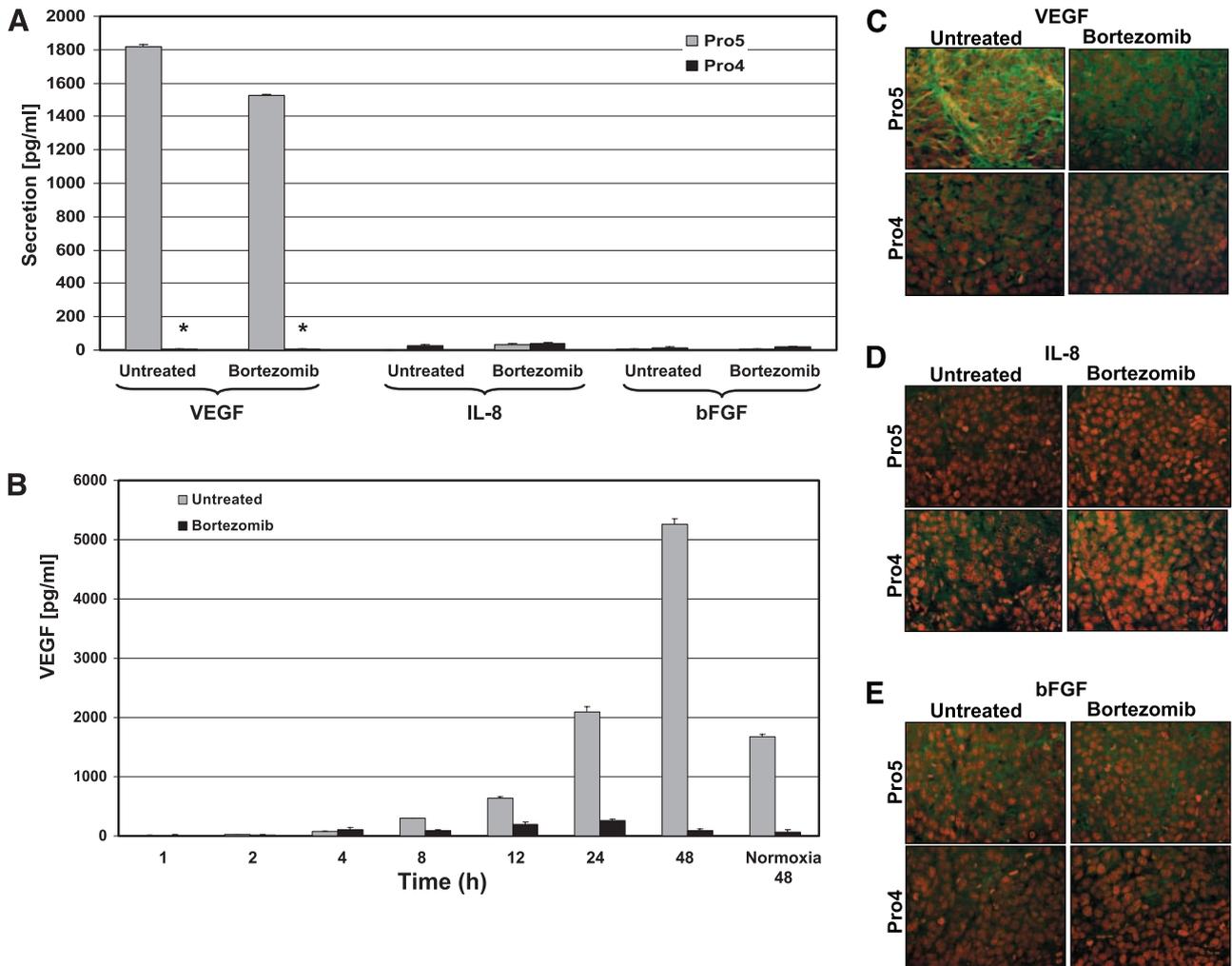
Figure 4. Effects of bortezomib on angiogenic factor production. **A,** baseline factor production *in vitro*. Levels of VEGF, IL-8, and bFGF were quantified in conditioned media obtained from cells treated with bortezomib for 8 h by ELISA. *Pro5,* LNCaP-Pro5; *Pro4,* PC3M-Pro4. Mean ± SD, $n = 3$. *, $P < 0.05$. **B,** time-dependent induction of VEGF secretion in LNCaP-Pro5 cells in response to hypoxia. Cells were incubated in a hypoxia chamber under an atmosphere of 1% O_2 in the absence or presence of bortezomib and VEGF secretion in conditioned medium was measured by ELISA. Cells incubated for 48 h under a normal atmosphere (*Normoxia*) served as controls. **C – E,** effects of bortezomib on tumor-associated production of angiogenic factors. Paraffin sections were stained antibodies specific for VEGF, IL-8, or bFGF, and factor levels were assessed by immunofluorescence as described in ''Materials and Methods.'' *Pro5,* LNCaP-Pro5; *Pro4,* PC3M-Pro4. **C,** effects on VEGF production. **D,** effects on tumor IL-8 levels. **E,** effects on bFGF levels. Sections shown are representative of results obtained in three high-power fields from each of three tumors (peripheral regions).

of established PC-3 tumors by more than 70%, presumably because some VEGF signaling is absolutely required for endothelial cell differentiation and survival. We are in the process of directly defining the role of p53 in this dichotomy using LNCaP-Pro5 cells that stably express the p53-inhibitory human papillomavirus E6 protein. We consider it likely that a large fraction of the tumor cell death observed in the bortezomib-treated LNCaP-Pro5 tumors resulted from indirect effects of the drug on the tumor vasculature.

Despite recent progress in defining the molecular alterations that contribute to prostate cancer progression and metastasis, there is general consensus that current therapeutic strategies are relatively inactive in patients with androgen-independent cancer. The results of this study and others demonstrate that bortezomib interferes with tumor cell proliferation and angiogenesis and induces apoptosis in tumors at clinically achievable concentrations of the drug. Bortezomib affects a number of different pathways important for tumor progression, including p53[2] and the transcription factor, NFκB (13). Dose escalation in the Phase I clinical trials conducted to date has been guided by biochemical assays of 20S proteasome activity in patent blood samples, and surprisingly little toxicity has been observed at doses of

---

[2] S. Williams and D. J. McConkey. The proteasome inhibitor bortezomib stabilizes a novel active form of p53 in human LNCaP-Pro5 prostate cancer cells, submitted for publication.
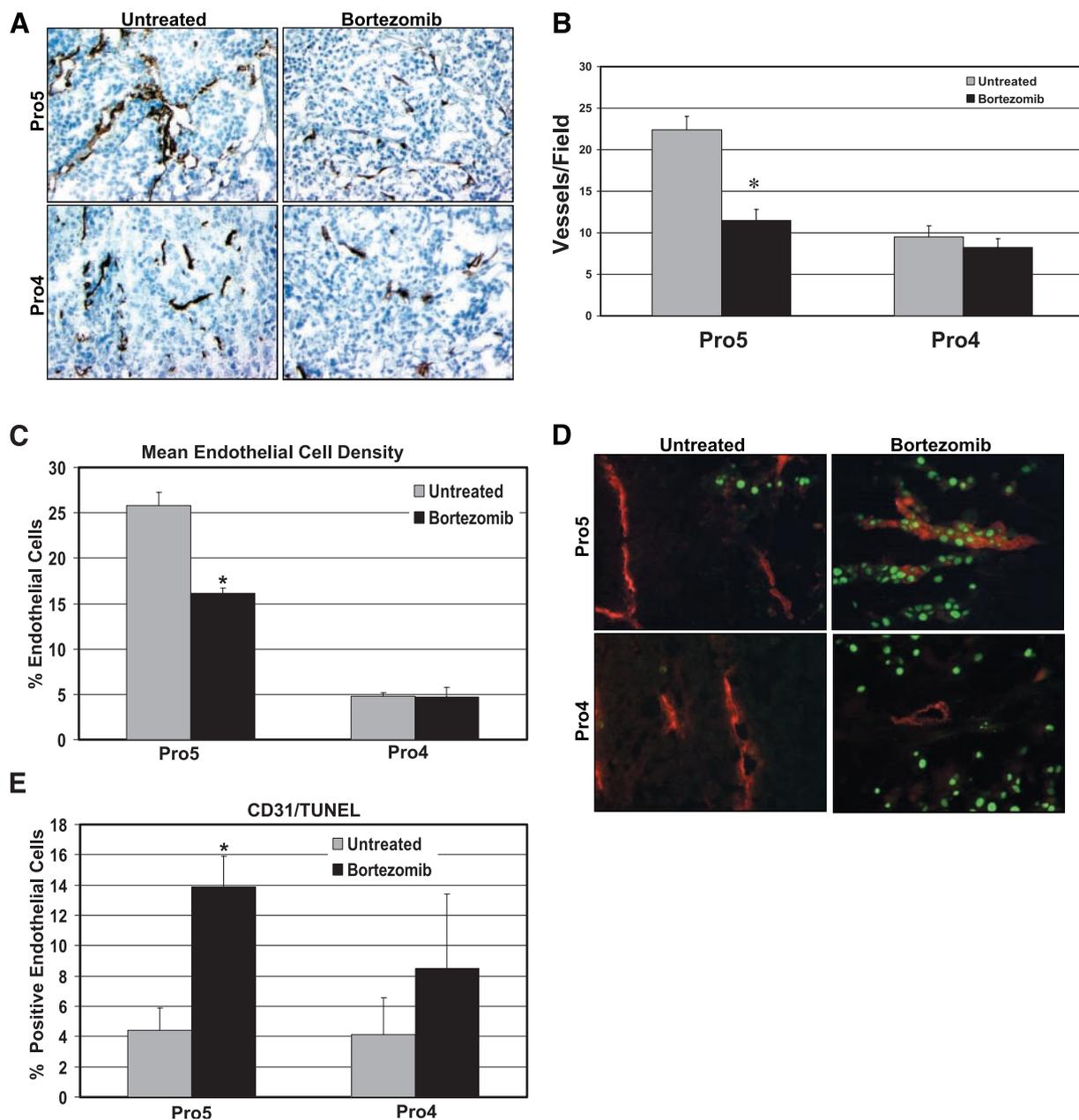
Figure 5. Effects of bortezomib on MVD and endothelial cell death. Frozen tissue sections were stained with antibodies to CD31 and/or DNA double-strand breaks by TUNEL. *Pro5,* LNCaP-Pro5; *Pro4,* PC3M-Pro4. **A,** colorimetric visualization of tumor microvessels by anti-CD31 immunohistochemistry. Sections were stained with an anti-CD31 antibody as outlined in ''Materials and Methods.'' Representative high-power fields are shown. **B,** quantification of tumor MVDs. Tumor sections were stained with an anti-CD31 antibody as described above, and tumor microvessels were counted in five representative peripheral high-power fields selected at random from three different tumors. Mean $\pm$ SD, $n = 5$. *, $P < 0.05$ *versus* controls. **C,** effects of bortezomib on mean endothelial cell density. The percentages of endothelial cells as fractions of total tumor cellular mass were determined by LSC as described in ''Materials and Methods.'' The rationale for using this method is that it standardizes for vessel size (assuming that larger vessels contain more cells). Mean $\pm$ SD, $n = 3$. *, $P > 0.05$. **D,** detection of dying endothelial cells by two-color immunofluorescence/TUNEL analysis. Sections were stained with immunofluorescent anti-CD31 and TUNEL as described in ''Materials and Methods.'' Nuclei were counterstained with Hoechst stain. Representative sections are shown. **E,** quantification of endothelial cell apoptosis. Percentages of CD31^{+}TUNEL^{+} cells were measured in four random fields from three different tumors using an LSC. Mean $\pm$ SD.

the drug that achieve target inhibition of 70–80% (11). As noted earlier, promising clinical activity has been observed in Phase I trials of bortezomib in androgen-independent prostate cancer, including reductions in serum PSA and IL-6 and radiological evidence of response. These properties make bortezomib an attractive candidate for combination with conventional agents for the therapy of advanced prostate cancer.

References

1. Ciechanover, A. The ubiquitin-proteasome proteolytic pathway. Cell, *79:* 13 – 21, 1994.

2. Goldberg, A. L. Functions of the proteasome: the lysis at the end of the tunnel. Science, *268:* 522 – 523, 1995.

3. Hochstrasser, M. Ubiquitin, proteasomes, and the regulation of intracellular protein degradation. Curr. Opin. Cell Biol., *7:* 215 – 223, 1995.

4. Goldberg, A. L., Stein, R., and Adams, J. New insights into proteasome function: from archaebacteria to drug development. Chem. Biol., *2:* 503 – 508, 1995.

5. Drexler, H. C. A. Activation of the cell death program by inhibition of proteasome function. Proc. Natl. Acad. Sci. USA, *94:* 855 – 860, 1997.

6. Drexler, H. C. A. Programmed cell death and the proteasome. Apoptosis, *3:* 1 – 7, 1998.

7. Grimm, L. M., Goldberg, A. L., Poirier, G. G., Schwartz, L. M., and Osborne, B. A. Proteasomes play an essential role in thymocyte apoptosis. EMBO J., *15:* 3835 – 3844, 1996.

8. Sadoul, R., Fernandez, P. A., Quiquerez, A. L., Martinou, I., Maki, M., Schroter, M., Becerer, J. D., Irmler, M., Tschopp, J., and Martinou, J. C. Involvement of the proteasome in the programmed cell death of NGF-deprived sympathetic neurons. EMBO J., *15:* 3845 – 3852, 1996.

9. Adams, J., Palombella, V. J., Sausville, E. A., Johnson, J., Destree, A., Lazarus, D. D., Maas, J., Pien, C. S., Prakash, S., and Elliott, P. J. Proteasome inhibitors: a novel class of potent and effective antitumor agents. Cancer Res., *59:* 2615 – 2622, 1999.

10. Adams, J. Proteasome inhibition in cancer: development of PS-341. Semin. Oncol., *28:* 613 – 619, 2001.

11. Adams, J. Proteasome inhibition: a novel approach to cancer therapy. Trends Mol. Med., *8:* S49 – S54, 2002.

12. Elliott, P. J. and Ross, J. S. The proteasome: a new target for novel drug therapies. Am. J. Clin. Pathol., *116:* 637 – 646, 2001.

13. Cusack, J. C., Jr., Liu, R., Houston, M., Abendroth, K., Elliott, P. J., Adams, J., and Baldwin, A. S., Jr. Enhanced chemosensitivity to CPT-11 with proteasome inhibitor PS-341: implications for systemic nuclear factor-κB inhibition. Cancer Res., *61:* 3535 – 3540, 2001.

14. Sunwoo, J. B., Chen, Z., Dong, G., Yeh, N., Crowl Bancroft, C., Sausville, E., Adams, J., Elliott, P., and Van Waes, C. Novel proteasome inhibitor PS-341 inhibits activation of nuclear factor-κB, cell survival, tumor growth, and angiogenesis in squamous cell carcinoma. Clin. Cancer Res., *7:* 1419 – 1428, 2001.

15. Nawrocki, S. T., Bruns, C. J., Harbison, M. T., Bold, R. J., Gotsch, B. S., Abbruzzese, J. L., Elliott, P., Adams, J., and McConkey, D. J. Effects of the proteasome inhibitor PS-341 on apoptosis and angiogenesis in orthotopic human pancreatic tumor xenografts. Mol. Cancer Ther., *1:* 1243 – 1253, 2002.

16. Teicher, B. A., Ara, G., Herbst, R., Palombella, V. J., and Adams, J. The proteasome inhibitor PS-341 in cancer therapy. Clin. Cancer Res., *5:* 2638 – 2645, 1999.

17. Pettaway, C. A., Pathak, S., Greene, G., Ramirez, E., Wilson, M. R., Killion, J. J., and Fidler, I. J. Selection of highly metastatic variants of different human prostatic carcinomas using orthotopic implantation in nude mice. Clin. Cancer Res., *2:* 1627 – 1636, 1996.

18. Nicoletti, I., Migliorati, G., Pagliacci, M. C., Grignani, F., and Riccardi, C. A rapid and simple method for measuring thymocyte apoptosis by propidium iodide staining and flow cytometry. J. Immunol. Methods, *139:* 271 – 279, 1991.

19. Davis, D. W., Buchholz, T. A., Hess, K. R., Sahin, A. A., Valero, V., and McConkey, D. J. Automated quantification of apoptosis after neoadjuvant chemotherapy for breast cancer: early assessment predicts clinical response. Clin. Cancer Res., *9:* 955 – 960, 2003.

20. Shaheen, R. M., Davis, D. W., Liu, W., Zebrowski, B. K., Wilson, M. R., Bucana, C. D., McConkey, D. J., McMahon, G., and Ellis, L. M. Antiangiogenic therapy targeting the tyrosine kinase receptor for vascular endothelial growth factor receptor inhibits the growth of colon cancer liver metastasis and induces tumor and endothelial cell apoptosis. Cancer Res., *59:* 5412 – 5416, 1999.

21. Bruns, C. J., Harbison, M. T., Davis, D. W., Portera, C. A., Tsan, R., McConkey, D. J., Evans, D. B., Abbruzzese, J. L., Hicklin, D. J., and Radinsky, R. Epidermal growth factor receptor blockade with C225 plus gemcitabine results in regression of human pancreatic carcinoma growing orthotopically in nude mice by antiangiogenic mechanisms [In Process Citation]. Clin. Cancer Res., *6:* 1936 – 1948, 2000.

22. Bruns, C. J., Solorzano, C. C., Harbison, M. T., Ozawa, S., Tsan, R., Fan, D., Abbruzzese, J., Traxler, P., Buchdunger, E., Radinsky, R., and Fidler, I. J. Blockade of the epidermal growth factor receptor signaling by a novel tyrosine kinase inhibitor leads to apoptosis of endothelial cells and therapy of human pancreatic carcinoma. Cancer Res., *60:* 2926 – 2935, 2000.

23. Herbst, R. S., Mullani, N. A., Davis, D. W., Hess, K. R., McConkey, D. J., Charnsangavej, C., O'Reilly, M. S., Kim, H. W., Baker, C., Roach, J., Ellis, L. M., Rashid, A., Pluda, J., Bucana, C., Madden, T. L., Tran, H. T., and Abbruzzese, J. L. Development of biologic markers of response and assessment of antiangiogenic activity in a clinical trial of human recombinant endostatin. J. Clin. Oncol., *20:* 3804 – 3814, 2002.

24. Chandra, J., Niemer, I., Gilbreath, J., Kliche, K. O., Andreeff, M., Freireich, E. J., Keating, M., and McConkey, D. J. Proteasome inhibitors induce apoptosis in glucocorticoid-resistant chronic lymphocytic leukemic lymphocytes. Blood, *92:* 4220 – 4229, 1998.

25. Delic, J., Masdehors, P., Omura, S., Cosset, J. M., Dumont, J., Binet, J. L., and Magdelenat, H. The proteasome inhibitor lactacystin induces apoptosis and sensitizes chemo- and radioresistant human chronic lymphocytic leukaemic lymphocytes to TNFα-initiated apoptosis. Br. J. Cancer, *77:* 1103 – 1107, 1998.

26. Herrmann, J. L., Briones, F., Jr., Brisbay, S., Logothetis, C. J., and McDonnell, T. J. Prostate carcinoma cell death resulting from inhibition of proteasome activity is independent of functional Bcl-2 and p53. Oncogene, *17:* 2889 – 2899, 1998.

27. Almond, J. B., Snowden, R. T., Hunter, A., Dinsdale, D., Cain, K., and Cohen, G. M. Proteasome inhibitor-induced apoptosis of B-chronic lymphocytic leukaemia cells involves cytochrome *c* release and caspase activation, accompanied by formation of an approximately 700 kDa Apaf-1 containing apoptosome complex. Leukemia, *15:* 1388 – 1397, 2001.

28. Graeber, T. G., Osmanian, C., Jacks, T., Housman, D. E., Koch, C. J., Lowe, S. W., and Giaccia, A. J. Hypoxia-mediated selection of cells with diminished apoptotic potential in solid tumours. Nature, *379:* 88 – 91, 1996.

29. Yu, J. L., Rak, J. W., Coomber, B. L., Hicklin, D. J., and Kerbel, R. S. Effect of p53 status on tumor response to antiangiogenic therapy. Science, *295:* 1526 – 1528, 2002.

30. Sweeney, P., Karashima, T., Kim, S. J., Kedar, D., Mian, B., Huang, S., Baker, C., Fan, Z., Hicklin, D. J., Pettaway, C. A., and Dinney, C. P. Anti-vascular endothelial growth factor receptor 2 antibody reduces tumorigenicity and metastasis in orthotopic prostate cancer xenografts via induction of endothelial cell apoptosis and reduction of endothelial cell matrix metalloproteinase type 9 production. Clin. Cancer Res., *8:* 2714 – 2724, 2002.

31. Wedge, S. R., Ogilvie, D. J., Dukes, M., Kendrew, J., Curwen, J. O., Hennequin, L. F., Thomas, A. P., Stokes, E. S., Curry, B., Richmond, G. H., and Wadsworth, P. F. ZD4190: an orally active inhibitor of vascular endothelial growth factor signaling with broad-spectrum antitumor efficacy. Cancer Res., *60:* 970 – 975, 2000.

32. Wedge, S. R., Ogilvie, D. J., Dukes, M., Kendrew, J., Chester, R., Jackson, J. A., Boffey, S. J., Valentine, P. J., Curwen, J. O., Musgrove, H. L., Graham, G. A., Hughes, G. D., Thomas, A. P., Stokes, E. S., Curry, B., Richmond, G. H., Wadsworth, P. F., Bigley, A. L., and Hennequin, L. F. ZD6474 inhibits vascular endothelial growth factor signaling, angiogenesis, and tumor growth following oral administration. Cancer, *62:* 4645 – 4655, 2002.